Experimental Study of Thermal Conductivity Reduction of Silicon-Germanium Nanocomposite for Thermoelectric Application

by

Hohyun Lee

B.S., Mechanical Engineering (2003)
Seoul National University

Submitted to the Department of Mechanical Engineering
in Partial Fulfillment of the Requirements for the Degree of
Master of Science in Mechanical Engineering

at the
Massachusetts Institute of Technology
February 2005

Signature of Author.....
Department of Mechanical Engineering
January 14, 2005

Certified by.....
Gang Chen
Professor of Mechanical Engineering
Thesis Supervisor

Accepted by.....
Lallit Anand
Chairman, Department Committee on Graduate Students

Experimental Study of Thermal Conductivity Reduction of Silicon-Germanium Nanocomposite for Thermoelectric Application

by

Hohyun Lee

Submitted to the Department of Mechanical Engineering
in Partial Fulfillment of the Requirements for the Degree of
Master of Science in Mechanical Engineering

Abstract

To improve the thermoelectric energy conversion efficiency of silicon germanium (SiGe), two methods were used to decrease the thermal conductivity by increasing phonon boundary scattering at interfaces. In the first method, SiGe alloys were annealed at a temperature higher than the melting point to increase the number of grain boundaries. In the second method, SiGe composites were made with nanosize silicon particles. For anncaled SiGe alloys thermal conductivity decreased by a factor of two while power factor remained the same value. For SiGe nanocomposite thermal conductivity decreased by a factor of four to that of bulk alloy, but electrical conductivity deteriorated. Future work will focus on increasing electrical conductivity while reducing the thermal conductivity.

Thesis Supervisor : Gang Chen

Title : Professor of Mechanical Engineering

Acknowledgements

First of all, I would like to express my deep-hearted gratitude to professor Gang Chen for his support and advice. I specially thank our co-workers at MIT and Boston College: Professor Dresselhaus, Professor Zhifeng Ren, Dr. Dezhi Wang, Ming Tang, Shankar Kunwar, and UROP student Justin Lai. Without them, I could not make any progress. I also give words of thanks to all of our smart lab mates, who were helpful whenever I encountered problems. Lastly, I should thank my family and Heejin for their endless love and support.

This project was supported by NASA. (RPCT NRA – Contract # NAS3-03108)

Contents

List of Figures

Chapter 1.

Introduction

Thermoelectricity is the direct energy conversion of energy between electricity and heat within a material.[1, 2] Thermoelectric devices are appealing because they are reliable without moving parts and environment-friendly. However, their efficiency needs to be improved if they are to be competitive with current energy conversion technology. Nanotechnology presents the possibility of enhancing thermoelectric efficiency. In this chapter, after a brief introduction to thermoelectrics, the main objectives of this thesis will be discussed.

1.1. Thermoelectrics

When a material is subjected to a temperature difference, an electrical potential difference is produced across the material. Conversely, when electrical current flows through a material, heat is also moved. These phenomena are called *thermoelectric effects*. Figure 1.1.1 shows the thermoelectric effects in a single material. More specifically, the former is called the *Seebeck effect* and the latter is called the *Peltier effect*, named after the

scientists who first observed these phenomena.[2]

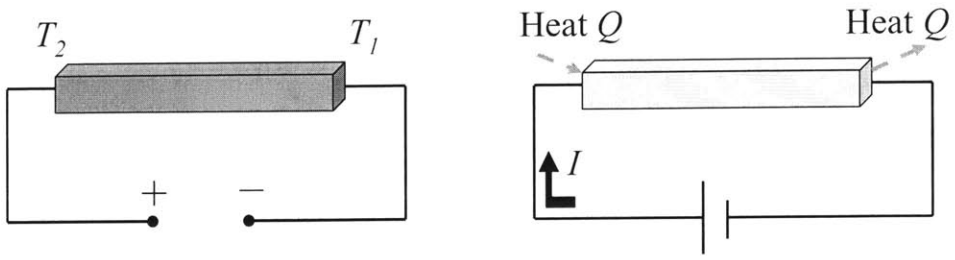

Fig. 1.1.1. Thermoelectric effects in a material. A temperature difference induces a voltage through the material, and current flow induces heat flow through the material.

The fundamental physical reason for thermoelectric phenomena is that charge carriers such as electrons and holes, are also heat carriers. When a material is subjected to a temperature gradient, charge carriers will diffuse from the hot side to the cold side. This diffusion brings about a higher electrical carrier concentration in the cold side and thus creates an electrostatic field and chemical potential gradient. The combined electrochemical potential creates an opposing current that balances the thermal diffusion. The *Seebeck coefficient* S is defined as the ratio of gradient of the Seebeck voltage to the temperature gradient.

$$S = -\frac{dV}{dT} \tag{1.1.1}$$

The negative sign is understandable because the Seebeck voltage is induced in the direction that resists thermal diffusion of electrical carriers by temperature gradient.

While the Seebeck effect is electrical potential difference caused by temperature gradient, Peltier effect is the transport of heat by electrical carrier flow. An electrical current is accompanied by a heat current because movement of electrical carriers involves

movement of entropy. The amount of heat flow Q is proportional to the electrical current I, and the proportionality constant is defined as *Peltier coefficient* Π.

$$\Pi = \frac{Q}{I} \tag{1.1.2}$$

When an electrical current flows around a loop with two dissimilar materials, the amount of energy flow abruptly changes at the junction due to the difference in Peltier coefficients. To satisfy energy conservation, the excess energy is liberated at one junction (heating) and the deficient energy is absorbed at another junction (cooling). The Peltier effect is reversible and depends on the direction of the current.

When the majority of electrical carriers are electrons, i.e, an n-type semiconductor, the Seebeck coefficient and the Peltier coefficient have negative values because direction of electron movement is opposite to that of current. On the other hand, when the majority of electrical carriers are holes, i.e., a p-type semiconductor, the Seebeck coefficient and the Peltier coefficient have positive values. Thermoelectric devices can be made with pairs of p-type and n-type materials. Typical schematics of thermoelectric devices are shown in Fig. 1.1.2.

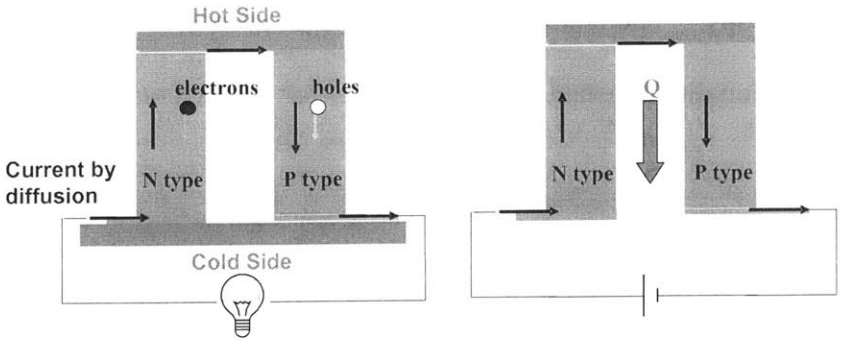

Fig. 1.1.2. Schematic of thermoelectric devices: power generator (left) and thermoelectric cooler (right)

Power generators and solid state refrigerators are good examples of thermoelectric devices that use the Seebeck effect and the Peltier effect respectively. The most typical applications of these devices are for deep-space exploration and mobile refrigerators. When a spacecraft travels far away from the sun, solar radiation is too weak to be used as an energy source. In this case, thermoelectric generators powered by nuclear energy units are often used to generate electricity. Small mobile refrigerators can be easily found in luxury cars. Since thermoelectric refrigerators do not require any moving parts nor coolants, they can be made small enough to be installed in cars.

Thermoelectric devices are reliable, as they do not require any moving parts that cause mechanical failure problem. They are also scalable, as their efficiency is not dependent on size of a system. Their application can vary from small integrated circuits to large power generators. Also, they are promising from the environmental point of view, as they are clean and quiet. No exhausts or wastes are produced for energy conversion. However, the efficiency of thermoelectric devices is too low to warrant their economic use in large scale power generators and refrigerators.

Thermoelectric efficiency is described by the dimensionless figure of merit, ZT, which is defined as

$$ZT = \frac{S^2 \sigma T}{k} \qquad (1.1.3)$$

where, S is the Seebeck coefficient, σ is electrical conductivity, k is thermal conductivity, and T is the operation temperature; the expression $S^2\sigma$ is called the *power factor*.[2] ZT being proportional to the square of the Seebeck coefficient is consistent with equation (1.1.1) because the efficiency is proportional to the amount of power generated and subsequently the power is proportional to the square of the voltage created by the Seebeck effect. It is also reasonable that ZT is proportional to electrical conductivity because high electrical conductivity reduces energy leakage by Joule heating within the material. On the other hand, a high thermal conductivity will decrease energy conversion efficiency, because a high thermal conductivity enhances heat transfer through the sample, and thus the temperature difference cannot be sustained. Finally, the equation is multiplied by the operation temperature to give it a nondimensionalized form. Since the Seebeck coefficient, electrical conductivity, and thermal conductivity depend on temperature, it is important to indicate at which temperature those properties are measured.

Therefore, good thermoelectric materials require a high Seebeck coefficient, a high electrical conductivity, and a low thermal conductivity. However, those three thermoelectric properties are not independent, so it is hard to change only one property without changing the others. For example, increasing the number of electrical carriers not only increases electrical conductivity but also increases thermal conductivity. Besides, the

Seebeck coefficient is inversely proportional to carrier concentration. Figure 1.1.3 shows each of three properties as a function of carrier concentration. As the figure shows, metals have high electrical conductivities, but also high thermal conductivities and low Seebeck coefficients. Insulators have high Seebeck coefficients and low thermal conductivities, but these properties are countered by low electrical conductivities. The best materials for thermoelectric applications are found in semiconductors. Moreover, in semiconductors electrical conductivities and carrier type can be easily changed without affecting other properties, simply by changing the doping type and doping concentration. With dopants, electrical conductivity of semiconductors can reach up to 10^5 S/m. Because the contribution of electrons to thermal conductivity is not large for semiconductors, a change in doping concentration has little effect on thermal conductivity.

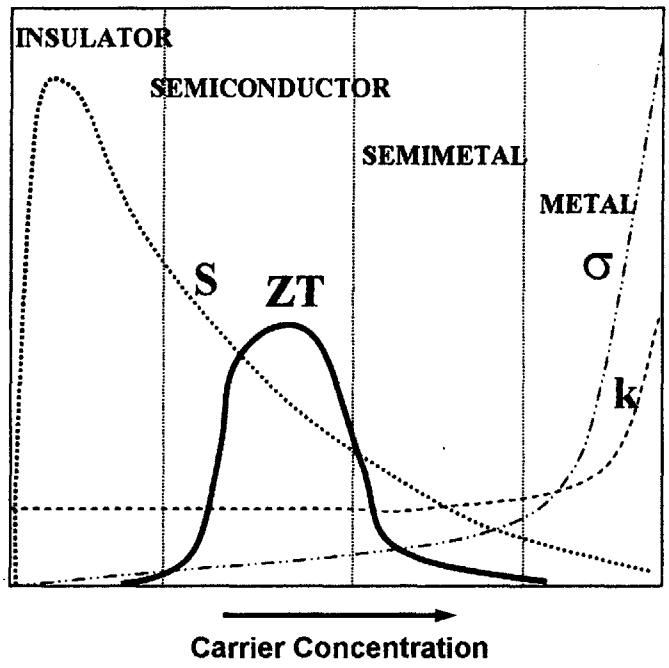

Fig. 1.1.3. Thermoelectric properties as a function of carrier concentration

During the 1950s, rapid progress was made on the development of alloy-based semiconductors. Because alloy decreases the thermal conductivity while maintaining the power factor, high thermoelectric figure of merit can be achieved. Among those materials, $Bi_{0.5}Sb_{1.5}Te_3$ was the most efficient p type thermoelectric material, with a *ZT* of 1 at room temperature.[1] However, the equivalent *ZT* for typical mechanical power generators or refrigerators is more than 3. In order for thermoelectric materials to be competitive with current energy conversion technology, more research was needed to enhance *ZT*. Between 1960 and 1990, there was not much progress in *ZT*. But in the last 10 years, significant enhancement in *ZT* has been made with the help of nanotechnology.[3]

In 1993, Hicks and Dresselhaus presented a possible enhancement in *ZT* through the use of quantum well superlattices and quantum wires.[4, 5] Figure 1.1.4 shows pictures of these nanostructures. Reduced dimensionality, as occurs in quantum well superlattices (2D) or in quantum wires (1D), enhances the density of states by quantum confinement, leading to an increase in the Seebeck coefficient without decrease in electrical conductivity.

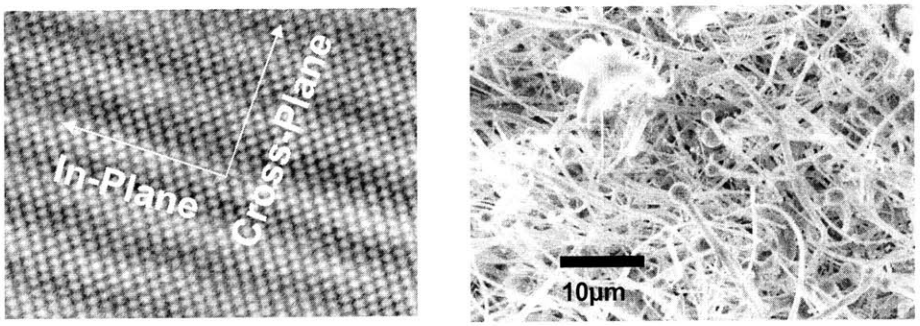

Fig. 1.1.4. Quantum well superlattice (left) and quantum wire (right). Each layer thickness in superlattice is 2 nm. Quantum well superlattice was made by Professor Wang's group at UCLA and quantum wire was made by Professor Ren's group at Boston College. Quantum confinement and boundary scattering are expected to result in the high Seebeck coefficient and low thermal conductivity without a decrease in electrical conductivity.

While the power factor increases in nanostructures, the thermal conductivity decreases. There are two differing explanations for the thermal conductivity reduction in low dimensionality. The first explanation treats phonon as a coherent wave just as in an electron wave.[6-10] Periodicity of nanostructures causes modification of phonon modes, and in turn reduces the phonon group velocity. Reduced phonon group velocity is proposed as an explanation for the thermal conductivity reduction in cross-plane direction of superlattices.[10] However, experimental results showed larger decrease in thermal conductivity than in the simulation results.[11-14] (Fig. 1.1.5) This fact suggests that modification in phonon modes alone cannot explain the thermal conductivity reduction in nanostructures. The alternate explanation treats phonon as incoherent particles and considers interface scattering as the classical size effect.[15-18] These approaches are based on solving the Boltzmann transport equation. They assume the thermal conductivity reduction comes from phonon scattering at boundaries. Phonons can easily scatter away

at every interface because the wavelength of phonons (1~2 nm at room temperature) is comparable to the length scale of surface roughness (3 Å at room temperature). On the other hand, the electrical conductivity is not significantly affected by boundary scattering because electrons have a longer wavelength (8 nm at room temperature) than phonons. With partially diffuse and partially specular interface scattering, modeling studies match well with experimental results. Thermal conductivity reduction by the classical size effect happens when the mean free path of phonon (100~200 nm at room temperature) is comparable to or larger than the characteristic length of structures.[15-17] Hence, increased amount of boundaries and not periodic structures in nanostructures is critical factor for thermal conductivity reduction.

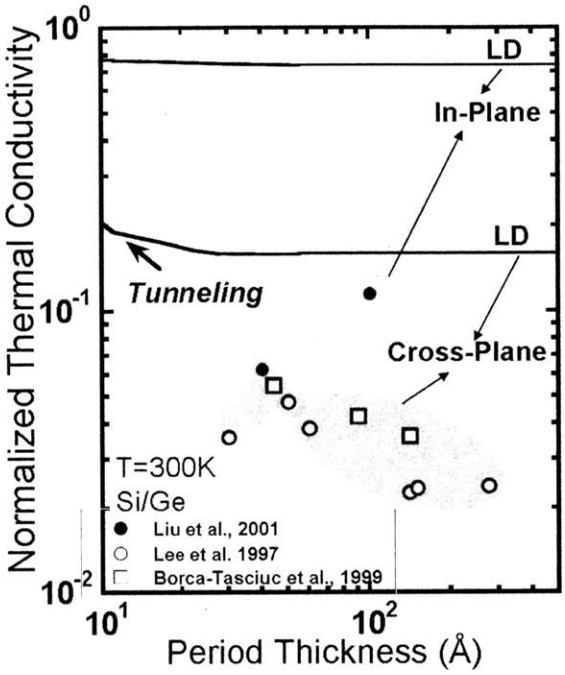

Fig. 1.1.5. Experimental and calculated thermal conductivity of SiGe superlattices in both in-pland and cross-plane, normalized to thermal conductivity of SiGe bulk alloy. Solid lines were calculated by lattice dynamics simualtion.[14] The experimental results are lower than the calculated results.[11-13]

Several subsequent experimental studies followed to prove the increase in *ZT* of nanostructures.[19-22] The highest *ZT* value of 2.4 at room temperature was observed for Bi_2Te_3/Se_2Te_3 superlattices.[21] However, these superlattices are not practical for use in thermoelectric products, because the time and cost of fabrication are not competitive enough for mass production.

1.2. Objectives and Outline

As we discussed in the previous section, thermoelectric devices are promising but their application is limited by its low efficiency. Recent research showed enhancement of

thermoelectric figure of merit by the help of nanostructures such as superlattices. However, such nanostructures are not profitable due to its high fabrication cost and time. In this thesis, cost and time effective methods for reducing the thermal conductivity of silicon germanium (SiGe) were tested, with the goal of improving the material's thermoelectric efficiency. If phonon boundary scattering plays a key role for thermal conductivity reduction, nanostructures like superlattices are not required. Based on the idea that the thermal conductivity of nanostructures can be decreased by increasing the amount of interfaces and hence the amount of phonon boundary scattering, methods to increase the amount of interfaces are developed.

Two different types of SiGe samples were prepared to observe a decrease in thermal conductivity while maintaining the power factor $S^2\sigma$. First, SiGe alloys like those that have been used in space applications were annealed at a temperature greater than the melting temperature of SiGe alloy. By this process, the samples melted slightly and reformed new boundaries. Second, SiGe composites were made of nanosized silicon particles. While alloy is a homogeneous mixture of atoms, nanocomposites are mixtures of nanoparticles. Simple mixture of nanoparticles can increase the amount of boundaries due to increased surface area. Both processes were expected to decrease thermal conductivity by increasing the number of interfaces at which phonon scatters, while maintaining electrical conductivity and increasing the Seebeck coefficient by the quantum confinement effect. All the samples were prepared with collaboration of Professor Ren's group at Boston College and Jet Propulsion Lab(JPL) at NASA.

SiGe was adopted in this research, because it has been the standard thermoelectric

material for power generation in spacecraft due to its high melting temperature. Although SiGe has a lower *ZT* than any other typical thermoelectric materials at room temperature, efficiency of an energy device increases with temperature. Figure 1.2.1 shows the thermoelectric figure of merit of various thermoelectric materials as a function of temperature.

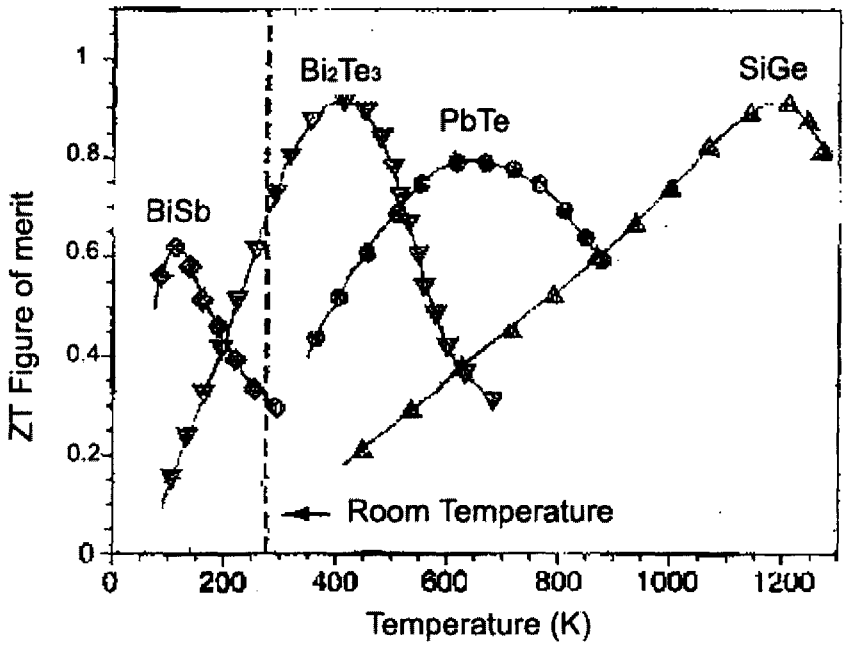

Fig. 1.2.1. Thermoelectric materials by temperature range.

Three thermoelectric properties, which are the thermal conductivity, the electrical conductivity, and the Seebeck coefficient, were measured for both types of samples. While these properties were measured, the measurement systems were also improved to give quick and reliable results. Chapter 2 will discuss the detail methods for sample preparation and for measurement technique. Then, measurement results and plans for the future work follow in Chapter 3 and 4 respectively.

Chapter 2.

Experimental Procedure

This chapter will discuss the experimental procedure, including sample preparation and thermoelectric properties measurement. Although there is a method for measuring *ZT* simultaneously, we have difficult in implementing it due to contact resistance.[23, 24] Individual properties should be measured separately because the change in each property can give us good direction for making good thermoelectric materials. However, thermoelectric properties measurements are time consuming and are easily affected by many factors. After defining the method for sample preparation, development in measurement techniques will be discussed. Tasks in section 2.1. were done by the Boston College group and the JPL group.

2.1. Sample Preparation

Two different fabrication methods for SiGe were explored to increase the amount of boundaries, hence to decrease thermal conductivity. First, SiGe alloy was heat treated at the temperature above the melting temperature, with expectation of new boundary creation.

Second, SiGe composites made of silicon nanoparticles were expected to have more grain boundaries due to reduced grain size. Detail procedures of these two methods are explained in the following sections.

2.1.1. Heat Treatment of SiGe Alloy

Usually, annealing process increases the size of grain boundaries, which in turn improves transport properties such as electrical conductivity and thermal conductivity.[25] In our case, a sample is heated up to the temperature below the solid line in the phase diagram of a material. Figure 2.1.1 shows the phase diagram of SiGe alloy. When the annealing temperature is over the solid line but below the liquid line, an alloy is expected to melt partially, starting from the grain boundaries, and form new boundaries after cooled down process. (Fig. 2.1.2) This idea was originally proposed by Professor Ren at Boston College, who is co-investigator for the project. This process is expected to create more boundaries than the original material, hence to have lower thermal conductivity.

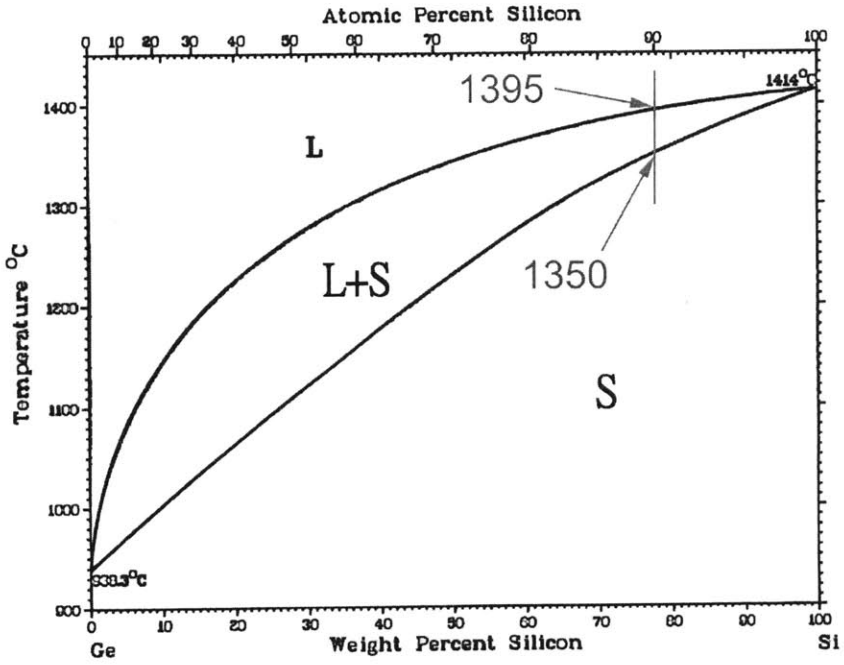

Fig. 2.1.1. Phase diagram of SiGe alloy with atomic percent and weight percent of silicon. Numbers indicate the temperatures of solid line and liquid line for $Si_{0.9}Ge_{0.1}$.

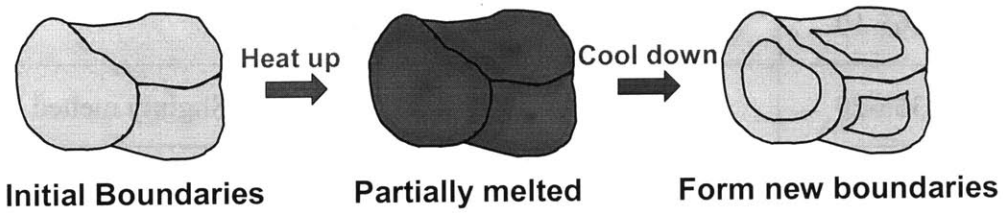

Fig. 2.1.2. Schematic of the annealing process at higher temperature than the solid line.

$Si_{0.9}Ge_{0.1}$, close to the composition of typical SiGe alloy for space application, was received from JPL, NASA and was heat treated for 10 minutes at the temperature between solid lines (1350℃) and liquid lines (1395℃). Heat treatment below the solid line was also made in order to observe the effect of annealing temperature. The processing information, such as annealing temperature, and time of the annealing, is summarized in Table 2.1.1. Heat treatment was also made at different holding time to observe any effect

of holding time.

Table 2.1.1. Heat treatment for $Si_{0.9}Ge_{0.1}$ alloy.

Sample Name	Annealed Temperature (℃)	Holding time (min)	Remarks
As Received 1			No heat treatment
As Received 2			No heat treatment
1345-10	1345	10	Under the solid line
1355-10	1355	10	
1360-5	1360	5	
1360-10	1360	10	
1360-20	1360	20	
1365-10	1365	10	
1365-20	1365	20	Slightly melted
1370-10	1370	10	
1375-10	1375	10	Melted a lot

Multi-purpose 1500℃ tube furnace from Lindberg Blue Company was utilized to reach high temperature. Temperature was controlled by built in PID controller. Temperature was set to be below 1375 °C because samples melted a lot over 1375 °C. Each sample was first sandwiched between two pieces of Si substrate. It is then enclosed inside a graphite sheet of thickness 0.13mm. The pressure range applied to the sample is 190~250 Torr, with a continuous flow of 400 sccm Ar gas to prevent the oxidation on the

surface.

2.1.2. SiGe Nanocomposites

Another approach to increase the amount of boundaries is by decreasing size of grain. By making composites from nanoparticles, we can expect small grain size. Commercially available nanosized silicon particles with micro-sized germanium particles were utilized to make nanocomposite. According to the current synthesizing technologies such as mechanical grinding and direct chemical synthesis, silicon is easier to make into nanosized particles than germanium. Hence, commercially available silicon particles can reach few tens of nm, while germanium particles are still in the range of ㎛. In addition to nanocomposite, composite with micron-sized silicon particles were also made to compare the effect of nano particles. Germanium of 100 mesh, which corresponds to 149 ㎛ of diameter, and silicon of 100 nm and 325 mesh, which corresponds to 44 ㎛ of diameter, were purchased from Alfa Aesar and Advanced Silicon Materials LLC.

Figure 2.1.3 shows the schematic of SiGe nanocomposites. The structures of nanocomposites could be the simple mixture of two particles or the silicon particles in the germanium host. The simple mixture structure (Fig. 2.1.3. left) seems more likely to occur in nature. However, for the easiness of simulation, structure of silicon particles in often adopted for modeling studies (Fig. 2.1.3. right).

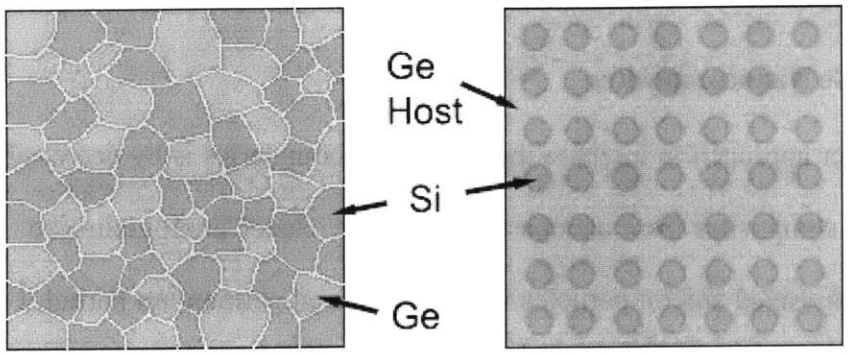

Fig. 2.1.3. Schematic of SiGe nanocomposite. It could be the simple mixture of silicon and germanium, (Right) or the silicon particles embedded in germanium host. (Left)

To ensure uniform distribution of silicon and germanium particles, the mixer at JPL was utilized to mix the particles. Figure 2.1.4 shows a mixer, which is similar to one we used.

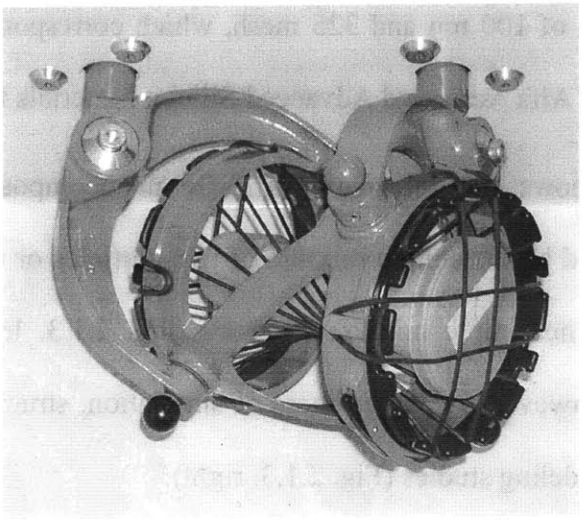

Fig. 2.1.4. A similar mixer that was used for mixing silicon and germanium particles. Particles are put inside of a bottle, and are mixed by rotation motion of the mixer.

After mixing properly, the mixed particles were hot pressed to make a pellet. The hot pressed process is important to attain a sample with high density. The appropriate

conditions, such as pressure and temperature, were determined by trial and error. Figure 2.1.5 shows the schematic of the hot press apparatus and Table 2.1.2 shows hot pressed conditions for each samples. Hot pressed temperature cannot be higher than the solid line. (Fig. 2.1.1) Two types of 1% Boron doped SiGe samples were prepared. One was $Si_{0.8}Ge_{0.2}$ and the other was $Si_{0.2}Ge_{0.8}$. They were prepared in order to check which composition has stronger size effect.

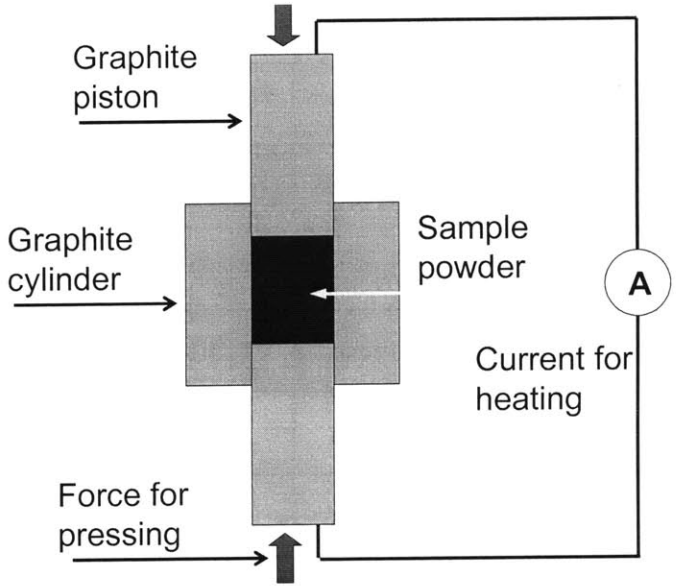

Fig. 2.1.5. Schematic of the hot press apparatus. A sample is placed on the middle of two pistons. And current is applied to heat the sample.

As seen in Table 2.1.2, hot press conditions are critical to have dense sample. Dense sample may be most desirable for thermoelectric application, because porous sample generally decreases electrical conductivity significantly. Only samples with high density were measured. Further experiments regarding optimized hot press condition could not be done due to lack of the samples.

Table 2.1.2. Table of hot pressed conditions for SiGe. Only shaded samples were measured due to reduction in electrical conductivity by porosity. Unit of mesh is number of sieve wires per inch. Equivalent particle diameters to 325 mesh and 100 mesh are 44㎛ and 149㎛ respectively.

Composition	Si particle diameter	Ge particle diameter	Temp. (℃)	Pressure (MPa)	Hold time	Density (%)
$Si_{80}Ge_{20}$	325 mesh	100 mesh	1000	127	5 min	85
$Si_{80}Ge_{20}$	325 mesh	100 mesh	1050	127	5 min	89
$Si_{80}Ge_{20}$	325 mesh	100 mesh	1050	127	5 min	90
$Si_{80}Ge_{20}$	325 mesh	100 mesh	1100	127	5 min	96
$Si_{80}Ge_{20}$	100 nm	100 mesh	1100	127	5 min	90
$Si_{80}Ge_{20}$	100 nm	100 mesh	1150	127	5 min	98
$Si_{20}Ge_{80}$	325 mesh	100 mesh	775	127	5 min	82
$Si_{20}Ge_{80}$	325 mesh	100 mesh	800	127	5 min	85
$Si_{20}Ge_{80}$	325 mesh	100 mesh	850	127	5 min	94
$Si_{20}Ge_{80}$	325 mesh	100 mesh	875	127	5 min	74
$Si_{20}Ge_{80}$	325 mesh	100 mesh	850	127	5 min	95
$Si_{20}Ge_{80}$	100 nm	100 mesh	850	127	5 min	83
$Si_{20}Ge_{80}$	100 nm	100 mesh	850	127	5 min	84

2.2. Electrical Conductivity Measurement

2.2.1. System Setup

Electrical conductivity is usually measured indirectly by resistivity ρ. The resistivity ρ can be found from the relation $\rho=AR/L$, where R is resistance, L is sample's length, and A is sample's cross sectional area. The resistance is deduced from the slope of voltage drop to current flow into the sample. (Fig. 2.2.1)

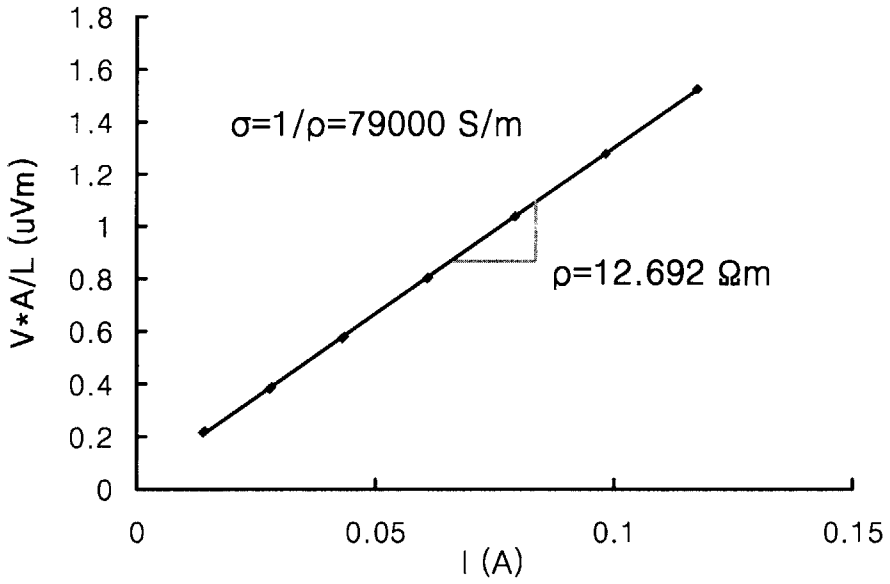

Fig. 2.2.1. Slope method for electrical conductivity.

Although electrical conductivity measurement technique has been developed to yield accurate results these days, there are still two problems for thermoelectric materials. One is a voltage by the Petlier effect, and the other is the contact resistance between the metal electrode and the semiconductor samples. Due to the Peltier effect, external current induces a temperature gradient. This temperature gradient in turn generates electrical potential difference, Seebeck voltage. The Seebeck voltage hinders the exact

measurement of voltage induced by the resistance of the sample. To avoid this effect, an AC current source was utilized to measure electrical resistance.[26] Since AC current alters direction periodically, there cannot be net temperature difference by the Peltier effect. Previous experimental study suggests that 60 Hz of the frequency is enough to neglect the Peltier effect.[24] We used 1 kHz, because of the stability problem of an AC current source.

Another problem with electrical conductivity measurement is the contact resistance. This contact resistance is due to the difference of the electron internal energy level between the metal and the semiconductor, called *Schottky Barrier*.[27] The contact resistance is also due to the oxide layer on the surface. The contact resistance can be as much as one hundred ohms. Resistance of samples is expected to be less than ten ohms. Reliable electrical conductivity data can be obtained only after the contact resistance problems have been solved. A four probe method[28] is typically used to eliminate the contributions of contact resistance. Current is injected through one set of current leads, and voltage is measured using another set of voltage leads. Because of high impedance of digital multi-meter, only voltage drop induced by current can be measured. Figure 2.2.2 shows a basic schematic of the electrical conductivity measurement system using the four probe method with AC current source.

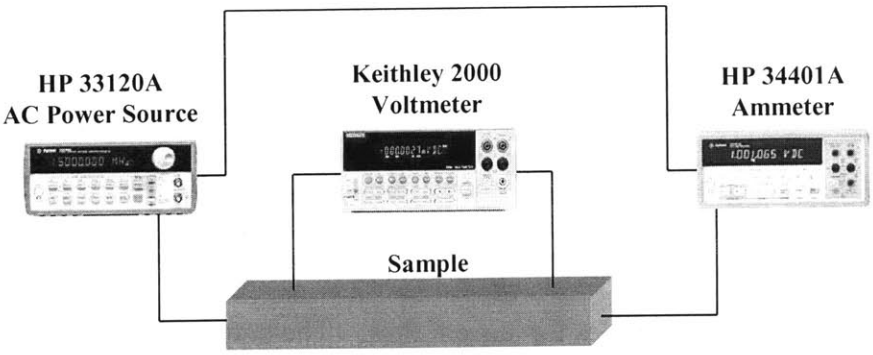

Fig. 2.2.2. Schematic of electrical conductivity measurement

Although the effect of contact resistance can be eliminated by the four probe method, inconsistent contact resistance leads to unstable result. Moreover, growth of the oxidation layer in the air can increase the contact resistance up to few tens of kilo-ohms. Methods for solving these problems were developed and will be discussed in the following sections.

2.2.2. Sample Holder

Intrinsic contact resistance, *Schottky Barrier*, is caused by the gap between the work function of the metal and the electron affinity of the semiconductor. It exists even in the zone where metal and semiconductor are in good physical contact. Resistance is high and unstable when two materials are not in good physical contact. Therefore, it is important to secure a stable contact between the metal probes and the semiconductor samples.

Resistance was found to be stable when probes touched the surface of a sample in constant pressure. Two solutions were suggested to apply a constant pressure. The first solution was to attach probes with silver paste from Epoxy Technology©. Although the silver paste could hold probes firmly during experiment, there existed uncertainty in length measurement between the two probes due to a large blob of the silver paste. Besides,

silver paste has a long hardening time and is time inefficient.

The other solution was to make a sample holder, by which probes touched a sample with constant pressure. Figure 2.2.3 shows the sample holder that was designed for the electrical conductivity measurement. A sample is put on the bottom plate (Fig. 2.2.3a) that consists of two copper electrodes for current flow. The bottom plate is then covered by the top plate (Fig. 2.2.3b), which contains two copper wires for voltage measurement. Constant pressure is achieved by having two screws that are used to hold both of the plates together (Fig. 2.2.3c). Alumina, which has a melting temperature of 2323 ℃,[29] is utilized as the body material both for insulation and for withstanding the high temperature.

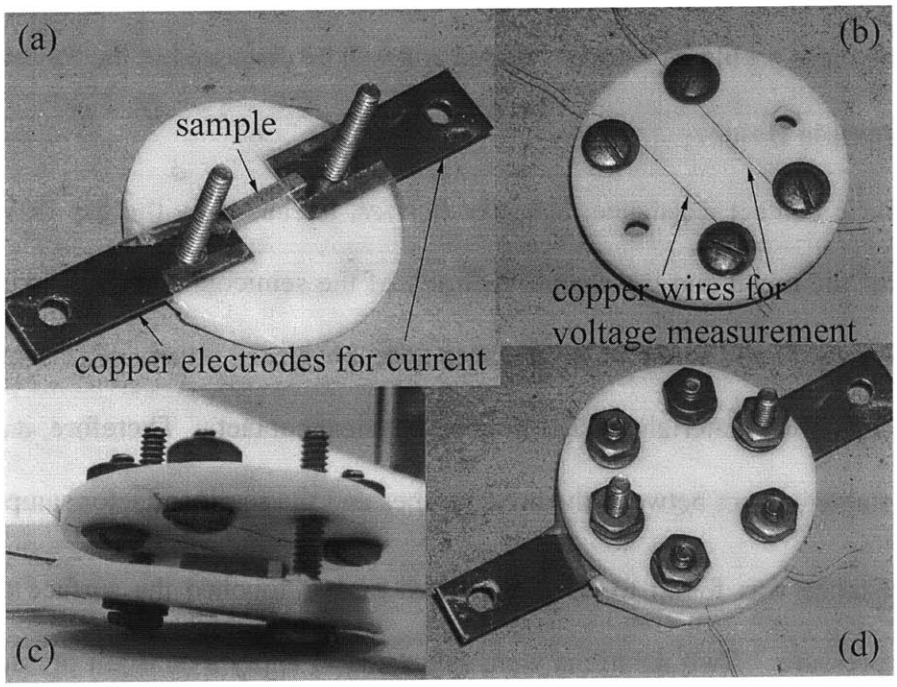

Fig. 2.2.3. A sample holder for electrical conductivity measurement. : (a) the bottom plate with a sample on it. (b) the cover plate which has two wires for electrical conductivity measurement. (c) combine two plates together. (d) use screws to apply constant pressure in order to acquire stable contact

Although one dimensional current flow may not be guaranteed with electrodes at the bottom (rather than at the ends), the bottom contact is advantageous to apply constant forces on the sample and thus stable contact resistance is acquired. The sample holder is also useful since it can reduce the measurement time and decrease the uncertainty in the length measurement. The electrical conductivity was measured for several samples with the help of this sample holder and results showed consistent values with a repeatability of 10% standard deviation.

2.2.3. Polishing System

Another contribution to contact resistance is the oxidation layer on the surface. The silicon germanium composite can be easily oxidized in the air even at the room temperature. Due to the dielectric nature of the oxide layer, oxidation layer of the silicon germanium composite needs to be removed before making electrical conductivity measurement. Silicon dioxide can be removed chemically by hydrofluoric acid, or mechanically by polishing the surface of a sample. Mechanical method was adopted due to a safety issue of the hydrofluoric acid. Polishing was also useful to have uniform dimensions of a sample.

Figure 2.2.4 shows a schematic of the polishing system. A two inch brass rod and a hub with a transition fit were designed. A sample is attached by wax on the top of the brass rod, and the hub guides a vertical position of the rod. 35 μm and 10 μm silicon Carbide powders and quartz plates from South Bay Technology, Inc. are utilized to polish the surface.

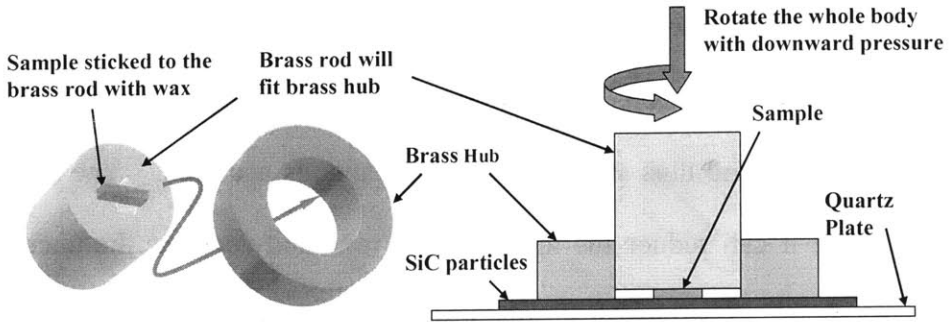

Fig. 2.2.4. Schematic of polishing system.

2.3. Seebeck Coefficient Measurement

The Seebeck coefficient measurement is known to be the easiest among the thermoelectric properties, because it is independent of geometric parameters and it is not sensitive to heat loss problem. The Seebeck coefficient S is defined as the ratio of the electrical potential difference ΔV to the temperature difference ΔT, $S=-\Delta V/\Delta T$. The temperature difference is determined by using K-type thermocouples, which are consisted of Alumel and Chromel.

Although the Seebeck coefficient measurement is not sensitive to the heat loss problem, unsteady heat loss is not desirable for good results. Because of an unwanted heat flow with any attachment to the sample, a sample holder cannot be used in this case to hold the thermocouples on a sample. On the other hand, the silver paste is used to make a contact between the thermocouples and the sample. Thermocouples with three milli-inch diameter are utilized to minimize conductive heat loss through thermocouples wires, and one branch of the thermocouples is used for voltage measurement. (Fig. 2.3.1)

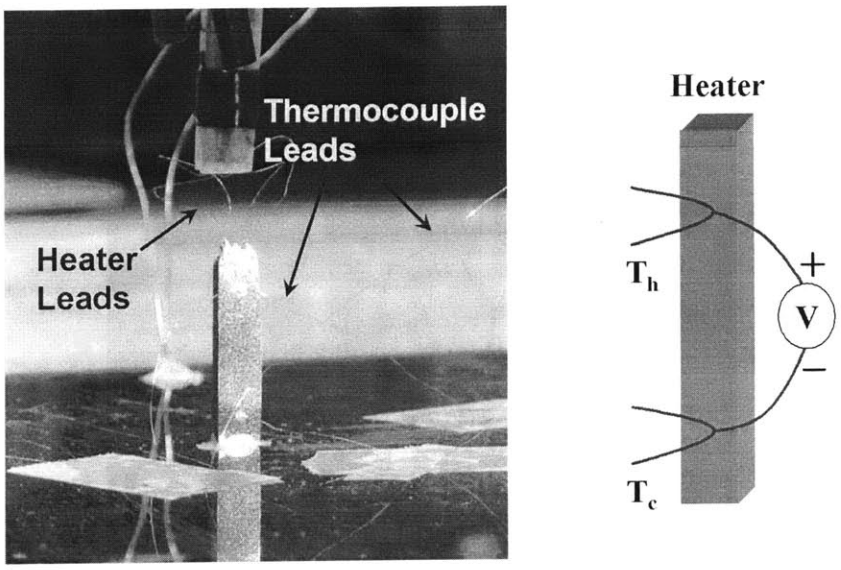

Fig. 2.3.1. Schematic of the Seebeck coefficient measurement system

Measurements are practiced under 10^{-5} torr vacuum in order to minimize temperature fluctuation due to convection. Figure 2.3.2 shows the vacuum system which is used for the Seebeck coefficient measurement and for the thermal conductivity measurement. Temperature difference is induced by an electric heater at the top of a sample as shown in Fig. 2.3.1. Six or seven data points were plotted in the ΔV-ΔT curve by changing the power that went through the electric heater. The Seebeck coefficient was acquired by a slope of the ΔV-ΔT curve, similar to electrical conductivity measurement case.

Fig. 2.3.2. Vacuum system for the Seebeck coefficient and thermal conductivity measurement system

One should note that the result should be compensated by the Seebeck coefficient of the wires that are used for voltage measurement. Since there exists temperature difference between the measurement points and ambient temperature, voltage drop by the wires affected the value of voltage measurement, $V = (T_\infty - T_h)S_w + (T_h - T_c)S_s + (T_c - T_\infty)S_w$ $= (T_h - T_c)(S_s - S_w)$. Hence, we should add the Seebeck coefficient of wires to the value we got from the slope. Both alumel and chromel wires were used for voltage measurements and the results were not different from each other. And experimental results show a repeatability of 4%.

2.4. Thermal Conductivity Measurement

Thermal conductivity k is defined as the ratio of heat flux q'' to the temperature gradient ∇T caused by the heat flux, $k=q''/\nabla T$. The same schematic we used for the

Seebeck coefficient can be applied for the thermal conductivity measurement. (Fig. 2.3.1) However, the thermal conductivity measurement is more difficult than the Seebeck coefficient or electrical conductivity because of heat loss problem. Unwanted heat flow happens mainly by radiative or convective heat loss from the surface and by unstable thermal contact between the heat source and the sample. The heat loss problems hinder the exact calculation of the heat flux that goes through the sample, and thus the exact thermal conductivity is unattainable. Therefore, minimizing unwanted heat flow is the most important thing in the thermal conductivity measurement. In the following sections, methods to decrease unwanted heat flow will be discussed.

2.4.1. Steady State Method

The steady state method is the most frequently used technique to determine thermal conductivity of bulk material.[30] As showed in Fig. 2.3.1, an electric heater (a heat source) is attached at the top of the sample that stands on a large copper plate. The copper plate works as a heat sink to ensure a one dimensional heat flow through the sample. Heat flux is calculated by the amount of power that goes through the electric heater divided by the cross sectional area. To get uniform heat flux, the sample must have a uniform cross sectional area. Uniform geometry can be acquired by using the polishing system mentioned in the previous chapter of electrical conductivity measurement.

The temperature is measured by K-type thermocouples at two points along an axial direction of a sample. Similar to the Seebeck coefficient measurement, 3 milli-inich thermocouples from Omega Engineering© are utilized to minimize conductive heat loss through the wires. By simple calculation, heat loss through the thermocouples wires are

expected to be less than 0.1% of total heat amount that goes through a sample.

When one dimensional heat flow in x-direction and linear temperature distribution are assumed along a sample, the relation $\nabla T = dT/dx = \Delta T/\Delta x$ can be valid. Then the thermal conductivity can be determined by slope of heat flux to temperature difference by using the relation $k=-q''\Delta x/\Delta T$. By changing the heat flux amount, several data points can be acquired. However, one should note that the assumption of linear temperature distribution is valid only when heat loss from the sample surface is negligible.

The heat loss from the sample surface is due to radiative and convective heat loss. Convective heat loss can be minimized by using the same vacuum system as in the Seebeck coefficient measurement. Radiative heat loss is simply calculated by average temperature of a sample surface T_{avg} and ambient temperature T_{amb} $q=\sigma\epsilon A(T_{avg}^4-T_{amb}^4)$, where σ is Boltzmann's constant and ϵ is emissivity of a sample. When the radiative heat loss is less than 1% of total heat that goes through a sample, it is appropriate to use the slope method. This slope method is valid for a sample of which thermal conductivity is more than 10 W/mK. However, radiative heat loss increases with increasing temperature, and with decreasing thermal conductivity and emissivity of a sample. Hence, the slope method cannot be applied in such conditions. Figure 2.4.1 shows that the assumption of linear temperature distribution cannot be hold with decreasing thermal conductivity. The figure is plotted by a fin model[29] which would be discussed later.

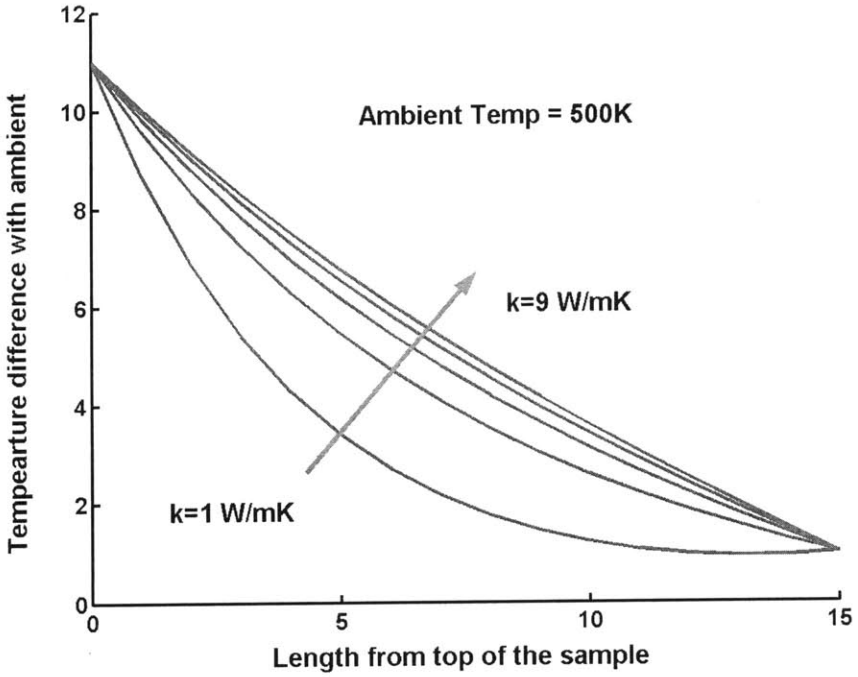

Fig. 2.4.1. Temperature distribution along a sample caused by steady state heat source at x=0 with the same temperature difference between x=0 and x=15cm. 500K ambient temperature is chosen because of visual clearness. Temperature distribution does not seem to be linear with decreasing thermal conductivity due to radiation loss from sample surface.

Two trials are made to minimize the radiative heat loss effect in the steady state method. The first trial is to make radiation shields outside of a sample. Although the radiation shields decreases the radiative heat loss, they cause another unwanted heat flow problem. Heat could be transferred from top to bottom by reflection from the shields. This problem is not good for calculating exact amount of heat flux. Figure 2.4.2 shows the sample with radiation shields, and its problem.

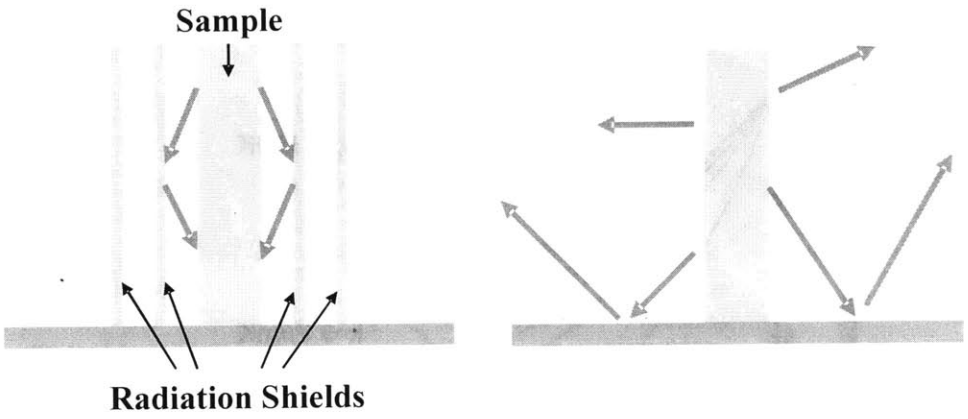

Fig. 2.4.2. A sample mounted on the copper plate with radiation shields and unwanted heat flow with radiation shields (Left). A sample mounted on the plate without a radiation shield. (Right)

The second trial is to calculate the thermal conductivity with consideration of radiative heat loss. In this case, it is better to let radiation go away without any radiation shield. As in the right of Fig. 2.4.2, radiation does not reflect back to the sample, so that we can assume a perfect absorbing ambient. With a perfect absorbing ambient, the fin model[29] can be applied. For one dimensional sample, from two temperatures heat can be determined by following equations.

$$q = \frac{hP}{m}\frac{(T_h - T_\infty)(e^{mL} + e^{-mL}) - 2(T_l - T_\infty)}{e^{mL} - e^{-mL}}$$
$$m = \sqrt{\frac{hP}{kA_c}}, h = 4\varepsilon\sigma T_\infty^{\ 3} \qquad (2.4.1)$$

where, q is heat that goes through a sample, A_c is cross sectional area of a sample, P is perimeter of cross section of a sample, L is a length between two thermocouples, T_h is temperature of higher point, T_l is temperature of lower point, T_∞ is ambient temperature, σ is Boltzmann's constant, ϵ is emissivity of a sample, and k is the thermal conductivity of a

sample. As the value of q can be calculated by the electrical power of electric heater, m can be solved from Eq. (2.4.1) using computer program. From the relation between m and k in equation (2.4.1), thermal conductivity k is derived. The result with this method is more accurate than the result with the slope method. However, because of thermal contact resistance between the electric heater and a sample, not all the electrical power goes through a sample. Power could be lost by radiation from the heater. And the amount of heat loss is difficult to estimate, because the temperature of the heater depends on how well the thermal contact was made. Besides, it is hard to estimate the sample emissivity. Therefore, for low thermal conductivity materials, we need to explore other measurement technique, which does not require a calculation of heat.

2.4.2. Transient Method

Throughout 19th and early of 20th century, non-steady-state methods to measure thermal transport property were developed both experimentally and mathematically.[31] Most of them measure thermal diffusivity rather than conductivity, which indirectly determines thermal conductivity with the value of specific heat and density.

$$k = \rho C \alpha \tag{2.4.2}$$

where ρ [kg/m^3] is density, C [J/kgK] is specific heat, and α [m^2/s] is diffusivity. The density can be easily determined by Archimedes' principle. We can use the well established result from a table[32] and a calculation[33] for the specific heat. And the diffusivity is acquired by solving one dimensional diffusion equation.

$$\frac{1}{\alpha}\frac{\partial T}{\partial t} + m^2 T = \frac{\partial^2 T}{\partial t^2} \tag{2.4.3}$$

where T is temperature difference to ambient temperature, and m is the coefficient of surface heat loss which takes into account heat loss by radiation, conduction, and convection. Depending on the boundary conditions, a wide range of solutions are possible.

In 1961, Angstrom developed the thermal diffusivity measurement method with sinusoidal heat source for a semi-infinite sample.[2, 34] And it has been modified and improved by numerous investigators and has become a well-established method for thermal diffusivity measurement.[35-37] Although Angstrom's method was established long time ago, it has not been properly replaced by other recent techniques due to its mathematical clearance and convenience of installation. Following is the mathematical derivation of how the thermal diffusivity is determined.

With sinusoidal heat source with a frequency ω mounted on the top of the sample (x=0), the solution of equation (2.4.3) is assumed to be in the form of

$$T(x,t) = A(x) + B(x)e^{i\omega t} \qquad (2.4.4)$$

where, i is the unit imaginary. In this equation only the $B(x)$ term, which is the amplitude of sinusoidal wave, matters for the derivation of the thermal diffusivity. The sinusoidal wave is realized by applying AC current to the electric heater in Fig. 2.3.1. When T of equation (2.4.3) is substitute by the T in equation (2.4.4), the second order ordinary differential equation for $B(x)$ becomes

$$B_{xx}(x) - (\frac{i\omega}{\alpha} + m^2)B(x) = 0 \qquad (2.4.5)$$

where B_{xx} is the second derivative of B with respect to x. The general solution of equation (2.4.5) is

$$B(x) = C_1 e^{\beta x} + C_2 e^{-\beta x}$$
$$\beta^2 \equiv m^2 + \frac{i\omega}{\alpha} \tag{2.4.6}$$

where C_1 and C_2 are constants to be determined by the following two boundary conditions. One of the boundary conditions is determined by the sinusoidal heat source,

$$T(x=0,t) = a + be^{i\omega t}$$
$$B(x=0) = b \tag{2.4.7}$$

Theoretically, the method we used for deriving the thermal diffusivity assumes semi-infinite sample for which the solution becomes

$$B(x) = be^{-\beta x} \tag{2.4.8}$$

When β is split into real part P and imaginary part Q, we can get the following relation.

$$PQ = \frac{\omega}{2\alpha} \tag{2.4.9}$$

And we can rewrite the solution of the diffusion equation as,

$$T(x,t) = A(x) + be^{-Px}\cos(\omega t - Qx) \tag{2.4.10}$$

From the equation, we can observe that amplitude and phase of sinusoidal temperature wave will be different from each measurement point. Measurements of only two temperature waves at two points $x=x_1$, x_2 are enough to determine the coefficients P and Q without knowing b. Hence, Angstrom method is useful in the sense that thermal diffusivity can be measured regardless of heat loss or amount of heat that goes through. Figure 2.4.3 shows a measurement result of the Angstrom's method.

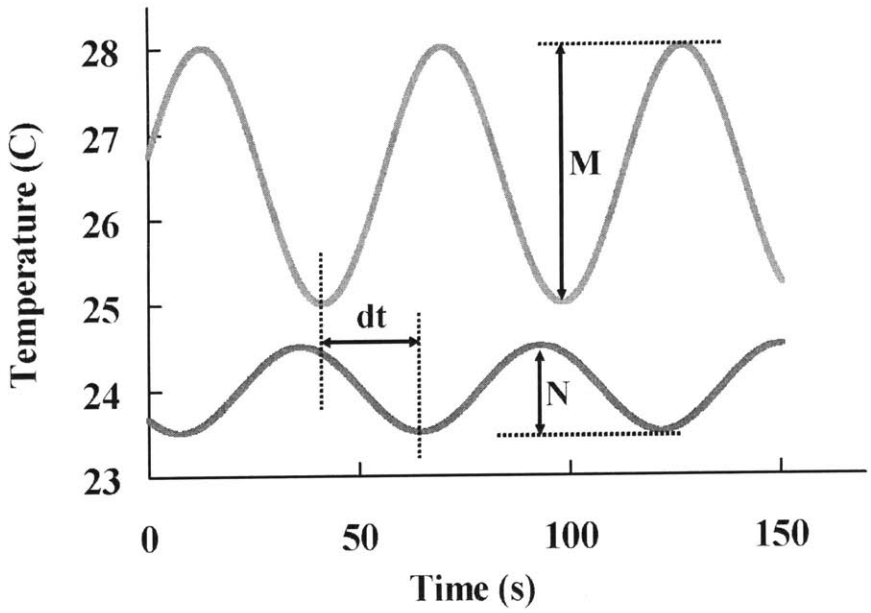

Fig. 2.4.3. Measurement result of Angstrom method. Temperature was measured at two points along a sample. Red one is at the upper thermocouples $x=x_1$ and Blue one is at the lower thermocouples $x=x_2$. M and N are the amplitudes of each signal, and dt is phase difference between signals.

From the measurement result, we can acquire amplitude M and N, and phase difference dt between two sinusoidal temperature waves. From two amplitudes, P in equation (2.4.10) can be determined.

$$\frac{M}{N} = \frac{be^{-Px_1}}{be^{-Px_2}} = e^{Pl}$$
$$P = \frac{1}{L}\ln\frac{M}{N} \qquad (2.4.11)$$

where, l is the length between two measurement points. And from phase difference Q is determined.

$$\begin{aligned} \omega t - Qx_1 &= \omega(t+dt) - Qx_2 \\ Q(x_2 - x_1) &= \omega \cdot dt \\ Q &= \frac{\omega \cdot dt}{l} \end{aligned} \tag{2.4.12}$$

With P and Q in equations (2.4.11) and (2.4.12), we can derive the thermal diffusivity α from equation (2.4.9)

$$\begin{aligned} PQ &= \frac{\varpi dt}{l^2} \ln\frac{M}{N} = \frac{\varpi}{2\alpha} \\ \alpha &= \frac{l^2}{2dt \ln\frac{M}{N}} \end{aligned} \tag{2.4.13}$$

By this relation, we can get thermal diffusivity without any knowledge of amount of power goes into a sample, and without any consideration of heat loss from sample surface.

However, the sample cannot be semi-infinite, but rather is finite with a length of L. Thus, the heat sink is attached at the bottom of the sample of length L $(x=L)$. With the heat sink, the temperature at $x=L$ should be close to the ambient temperature. With this boundary condition, the general form of $B(x)$ in equation (2.4.6) can be specified as

$$B(x) = b\left(\frac{e^{\beta x}}{1-e^{2\beta L}} + \frac{e^{-\beta x}}{1-e^{-2\beta L}}\right) \tag{2.4.14}$$

If equation (2.4.14) is not much different from equation (2.4.8), then the simple semi-finite method is still valid even for a sample with finite length. To meet this condition, the first term of equation (2.4.14) should be negligible and the denominator of the second term of equation (2.4.14) should be 1. That is, the real part of $2\beta L$ should be much greater than 1.

$$\mathrm{Re}(2\beta L) >> 1 \Leftrightarrow L >> \frac{1}{2\,\mathrm{Re}(\beta)} \qquad (2.4.15)$$

With a 10 W/mK magnitude for the thermal conductivity, a sample of 2 mm diameter, and a low heat source frequency such as 10 mHz, calculations show that L for the sample should be much longer than 1mm in order for the semi-infinite method to be valid. The lengths of the samples that were used for the measurement were around 12 mm, which can be thought of long enough. Figure 2.4.4 shows the dimensionless form of $B(x)/b$ with x given by equations (2.4.8) and (2.4.14). There is hardly any recognizable difference between the two lines.

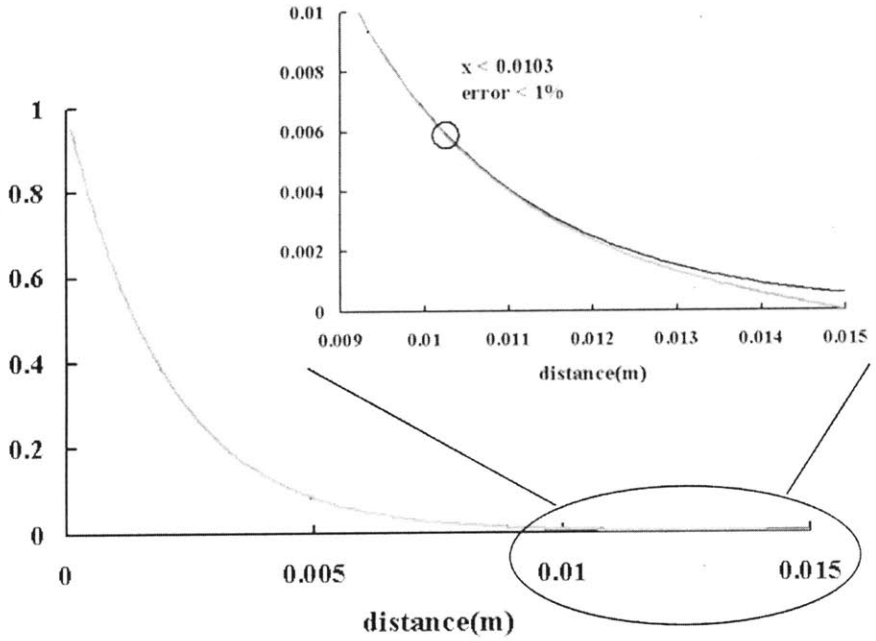

Fig. 2.4.4. Theoretical solutions of the amplitude of sinusoidal temperature for the case of β=500 m^{-1} with increasing distance from the heat source. Two different solutions with different boundary conditions are plotted in the same viewgraph. The two solutions give almost identical results. The difference between two graphs is growing larger than 1 % from x=0.0103 m.

However, with a closer look, from the point of 10.3 mm out of 15 mm sample, the error between two lines grows larger than 1 %. The error even more decreases with low wave frequency, low thermal conductivity, and low ambient temperature. Therefore, Angstrom's method is still valid for a finite sample with low thermal conductivity, as far as two thermocouples are attached above 5 mm from the bottom.

Pyrex Borosilicate glass was also utilized this time to calibrate the system. We used frequencies of 5mHz and 10mHz for the calibration and for the actual measurement. Although the pyrex glass was not a standard thermal conductivity reference material of the National Institute of Standards and Technology (NIST), this material is known to have quite a stable thermal conductivity value which is given in the literature to be around 1.14 W/mK. The experiment using the Angstrom method led to a value of 1.07±0.07 W/mK. Hence the reliability of the measurement system was around 7 % with repeatability of 6.5 %. The main sources of error in the thermal diffusivity measurement are uncertainty in the length measurement, the curve fitting, the value of the specific heat and density, and the defects of the sinusoidal power source. Similar to the steady state method, uncertainty in the length measurement between the two thermocouples exists for both methods. However, this effect is now more pronounced with the new method since thermal diffusivity is proportional to the square of l. Although the Angstrom method has various source of uncertainty, it showed better reliability and repeatability than the steady state method.

Chapter 3.

Results & Discussion

3.1. Heat Treated Samples

Heat treated samples showed reduction in thermal conductivity, and increase in the Seebeck coefficient without significant decrease in electrical conductivity. The detail measurement results are shown in Table 3.1.1 at the last part of this section. Some of the samples were not in good condition to carry out enough amount of measurement for the systematic data. The samples were in bad condition for measurement when they were treated at high temperature and for long holding time. However, we could observe a trend of change in thermoelectric properties with the heat treatment temperature. Change in each property will be discussed separately.

As in Fig. 3.1.1, the thermal conductivity reduced more or less throughout the annealing temperature region with 10 minutes holding time. The maximum reduction by the factor of two was observed in the annealing temperature region between 1360 ℃ and 1365 ℃. Although the temperature was not an actual annealed temperature but a value of

the furnace panel, it was supposed that there would not be more difference than 10 ℃ between the actual annealed temperature and the value of the furnace panel. Therefore, we can conclude that partial melting happened and another grain was formed at the temperature region slightly higher than a solid line. This conclusion can be supported by the result at the high temperature region. At high annealing temperature, samples melted a lot such that additional boundaries could not be formed. Increased amount of grain resulted in the reduction in the thermal conductivity due to boundary phonon scattering. The result was quite encouraging as not any previous study had shown decrease in thermal conductivity by a single heat treatment method.

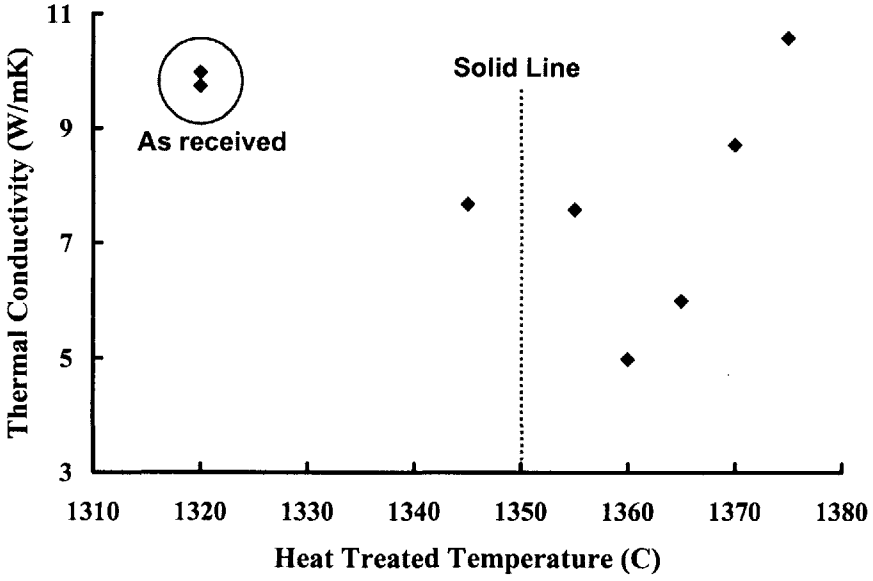

Fig. 3.1.1. Thermal conductivity (W/mK, y-axis) of the samples after 10 minutes of heat treatment at each temperature (℃, x-axis). Dashed line is solid line temperature. (1350 ℃)

Heat treatments with different holding time were carried out for the temperature region where we observed the biggest reduction in the thermal conductivity. Samples were heat

treated with the holding time of 5 and 20 minutes at 1360 ℃ and 1365 ℃. However, we could not observe further decrease in thermal conductivity. (Table 3.1.1) The sample heat treated at 1360 ℃ for 20 minutes showed satisfactory decrease in thermal conductivity, but the sample heat treated at 1365 ℃ for 20 minutes and the sample heat treated at 1360 ℃ for 5 minutes showed the same or increased value compared with the "as received" samples. 5 minutes with 1365 ℃ were broken so that it could not be measured. Systematic study should be carried out to decide the best condition for the heat treatment in the near future.

Figures 3.1.2 and 3.1.3 show the measurement results of the Seebeck coefficient and electrical conductivity respectively. While the Seebeck coefficient slightly increased or maintained compared with the "as received" samples, electrical conductivity slightly decreased after the heat treatment. However, as in Fig. 3.1.4, the power factor, which is product of square of the Seebeck coefficient and electrical conductivity, remained almost same for heat treated sample with holding time of 10 minutes. Hence, it is the thermal conductivity that decides the thermoelectric figure of merit, *ZT*.

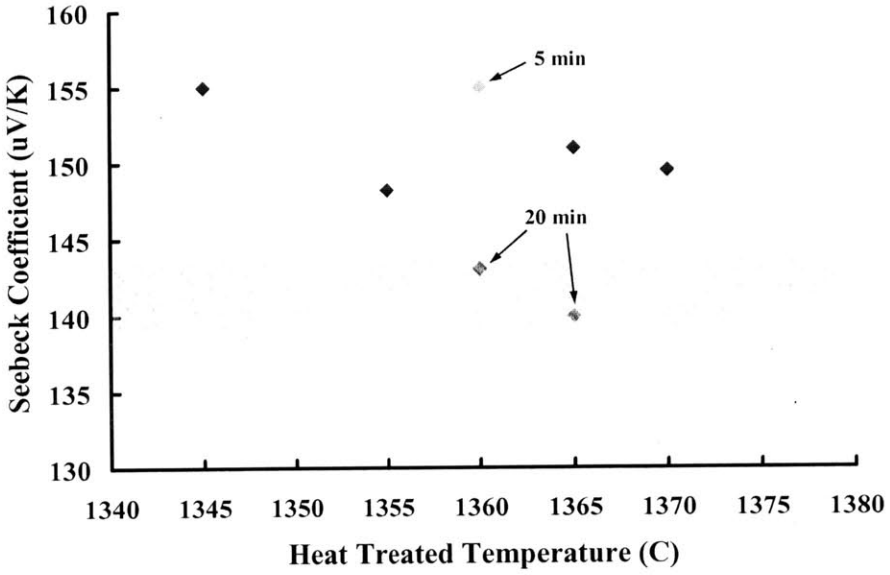

Fig. 3.1.2. Seebeck coefficient (μV/K, y-axis) of the samples after heat treatment at each temperature (℃, x-axis). Hold time was 10 minutes except for the samples indicated in the figure. Slanted red dashed lines denote the Seebeck coefficient range of the "as received" materials before heat treatment. Most of heat treated sample showed the Seebeck coefficient not worse than "as received" samples.

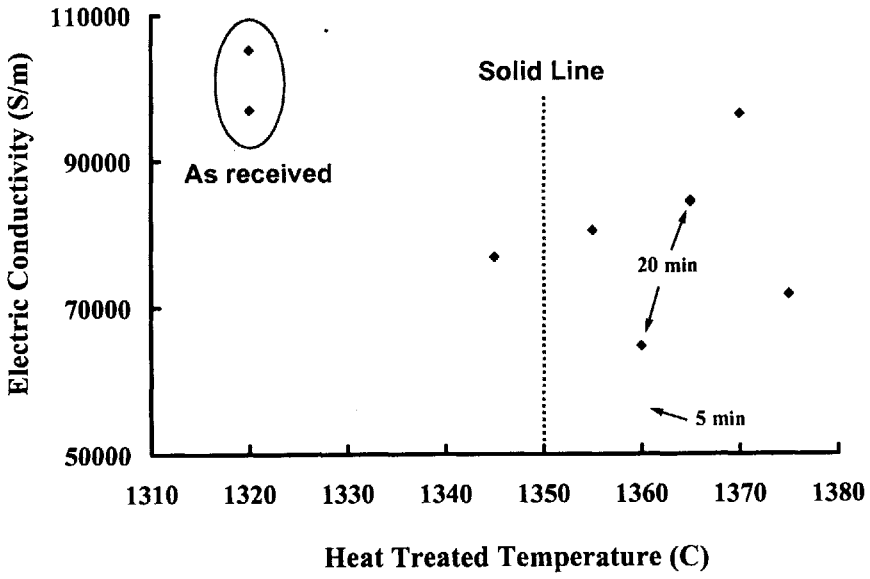

Fig. 3.1.3. Electrical conductivity (S/m, y-axis) of the samples after heat treatment at each temperature (℃, x-axis). Hold time was 10 minutes except for the samples indicated in the figure. Dashed line is solid line temperature. (1350℃) Electrical conductivity of heat treated samples did not reduced significantly.

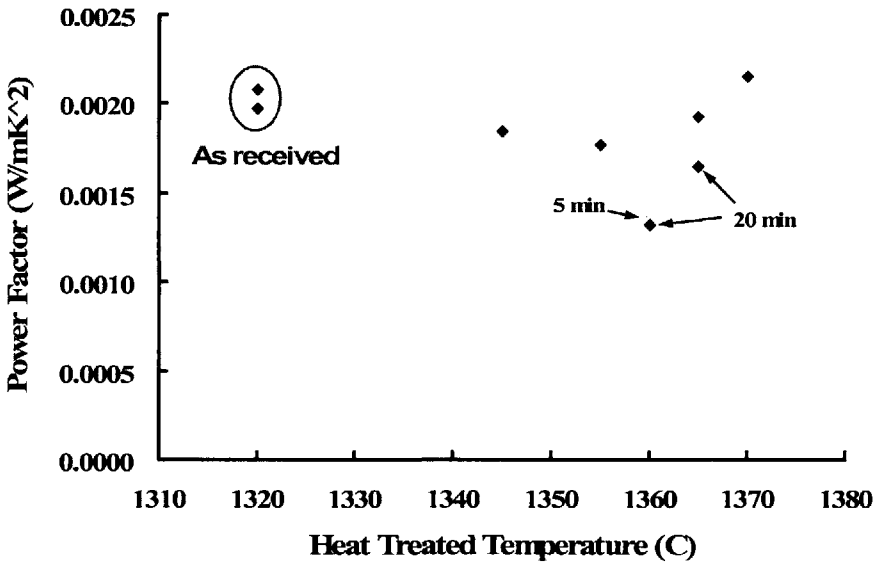

Fig. 3.1.4. Power factor (W/mK^2, y-axis) of the samples after heat treatment at each temperature (℃, x-axis). Hold time was 10 minutes except for the samples indicated in the figure. Power factor remained almost same for the heat treated samples with holding time of 10 minutes.

The best thermoelectric sample was 1365-10 with *ZT* of 0.096. (Table 3.1.1) *ZT* increase 57 % to "as received" samples. Unfortunately, the sample with the minimum thermal conductivity, "1360-10", was broken so that we could not observe the *ZT* for that sample. Although there still need more systematic experiments, we could conclude that heat treatment is a promising method in enhancing *ZT*.

Table 3.1.1. Room temperature measurement result of heat treated $Si_{0.9}Ge_{0.1}$ alloy.

Sample Name	Thermal Conductivity (W/mK)	Seebeck coefficient (μV/K)	Electrical conductivity (S/m)	*ZT*
As Received 1	9.97±0.45	143	95400	0.059
As Received 2	9.73±0.35	140	105200	0.063
1345-10	7.67±0.37	155	76800	0.072
1355-10	7.58±0.37	148	80400	0.070
1360-5	9.98±0.21	155	56200	0.041
1360-10	4.98±0.05	Broken	Broken	NaN
1360-20	6.56±0.50	143	64600	0.060
1365-10	6.00±0.39	151	84500	0.096
1365-20	12.0	140	84300	0.041
1370-10	10.6	150	96300	0.061
1375-10	8.71	95.1	71700	0.022

3.2. SiGe Nanocomposites

Table 3.2.1 shows the thermoelectric properties measurement results of SiGe nanocomposite. Although there are not enough data to conclude, thermal conductivity was lower in the samples with nanosized silicon particles than with micro-sized silicon particles. The comparison was made within the same composition and the same density

range. Moreover, the lowest thermal conductivity of 1.66 W/mK shows that the nanocomposite approach is quite promising, as this value is comparable with the lowest value of 1.4 W/mK ever measured in SiGe superlattice.[12]

Table 3.2.1. Room temperature measurement result of SiGe nanocomposite

Composition	Si particle diameter	Density (%)	Thermal Cond. (W/mK)	Seebeck Coeff. (μV/K)	Electric Cond. (S/m)	ZT
$Si_{80}Ge_{20}$	325 mesh	90	4.27±0.34	233	4000	0.015
$Si_{80}Ge_{20}$	325 mesh	96	5.94±0.48	110	74000	0.046
$Si_{80}Ge_{20}$	100 nm	90	1.66±0.14	250	3200	0.036
$Si_{80}Ge_{20}$	100 nm	98	4.27±0.29	104	89000	0.067
$Si_{20}Ge_{80}$	325 mesh	95	30.7±3.46	572	140	0.0004
$Si_{20}Ge_{80}$	100 nm	83	5.07±0.27	226	3800	0.012

Electrical conductivity was greatly reduced with decreasing density except for germanium rich composite. Although there are not enough data to conclude something, reduction in electrical conductivity was attributed to unactivated dopants as well as porosity effect. Similarly, before attributing the thermal conductivity reduction to size effect, we need to verify if there is any effect of porosity to thermal conductivity. The models for thermal conductivity reduction caused by porous effect were developed by Eucken and Russell in the early of 20th century.[38] The ratio of the thermal conductivity of porous media k_{porous}, to the thermal conductivity of solid media k_{solid}, can be described as,

$$\left(k_{porous}/k_{solid}\right)_{Eucken} = (1-\phi)/(1+\phi/2) \tag{3.2.1}$$

$$\left(k_{porous}/k_{solid}\right)_{Russell} = \left(1-\phi^{2/3}\right)/\left(1-\phi^{2/3}+\phi\right) \tag{3.2.2}$$

where, ϕ is porosity, which is equivalent to one subtracted by density ρ. By the equations (3.2.1) and (3.2.2), thermal conductivity reduction from the value of the SiGe bulk alloy was calculated. The thermal conductivities of $Si_{0.8}Ge_{0.2}$ and $Si_{0.2}Ge_{0.8}$ bulk alloys are 6.3 W/mK and 11.3 W/mK respectively.[32] Table 3.2.2 shows the calculation results of effective thermal conductivity by porous effect for the SiGe composite samples with nanosized silicon particles. From Table 3.2.2, we can conclude that the thermal conductivity has reduced more than by porous effect. However, recent study in our group suggests that nanosized porous can cause more reduction in thermal conductivity than macrosized porous. More study about nanosized porous effect must be explored in the near future.

Table 3.2.2. Effective thermal conductivity of SiGe nanocomposite by porous effect. Nanocomposites were made with 100nm silicon particles and 100mesh germanium particles. Calculations were made with both Eucken and Russell models.

Composition	Density (%)	Eucken model (W/mK)	Russell model (W/mK)	Measured value (W/mK)
$Si_{80}Ge_{20}$	90	5.4	5.6	1.66±0.14
$Si_{80}Ge_{20}$	98	6.1	6.2	4.27±0.29
$Si_{20}Ge_{80}$	83	8.6	9.1	5.07±0.27

The results in Table 3.2.2 suggested another fact that more decrease in thermal

conductivity happened for the low density sample than the high density sample. This is related with the hot press parameter, such as hot press temperature and holding time. With higher hot press temperature, high density sample could be acquired. But high temperature can grow grain size, just as in the case of normal annealing, so that boundaries were formed less than low temperature hot press. Hence, significant decrease in thermal conductivity could not be observed at 98% silicon rich nanocomposite as in the 90% silicon rich nanocomposite.

Germanium rich samples were prepared with the expectation of low thermal conductivity and high electrical conductivity, as bulk germanium particles have lower thermal conductivity and higher electrical conductivity than bulk silicon particles.[32] However, the experimental results showed the opposite case. The $Si_{20}Ge_{80}$ sample with 325 mesh of silicon particles showed the properties values that was even far higher than the values of bulk alloy. There could be problems with sample preparation procedure such as mixing or hot press. Besides $Si_{20}Ge_{80}$ with micro-sized silicon particles, $Si_{20}Ge_{80}$ with nanosized silicon also showed higher thermal conductivity than the silicon rich samples. Hence, it is not a thermal conductivity of bulk material that decides the thermal conductivity in nanostructures. This was also supported by a modeling study.[39] Yang suggested that silicon rich nanocomposite would have lower thermal conductivity than germanium rich nanocomposite by modeling study for SiGe nanocomposites.

The fact that the thermal conductivity of the composite with 100nm silicon was lower than that of the comoposite with 325 mesh silicon was expectable by many recent modeling studies on the thermal conductivity of superlattices and thin film.[15-17] Most of them

simulated the thermal conductivity reduction by diffuse phonon scattering at interfaces using Boltzmann Transport Equation. One of the modeling studies showed that thermal conductivity of in plane superlattices reduced with decreasing characteristic length of nanostructures. And the reduction was even more conspicuous when the characteristic length of nanostructures was comparable to or less than phonon mean free path. The bulk phonon mean free path is between 100 and 200 nm at room temperature.[40] Although these modeling studies were for superlattices, we can have physical sense that thermal conductivity reduced more in nanocomposite with 100 nm silicon particles than in composite with 325 mesh silicon particles.

Chapter 4.

Conclusions and Future Plans

4.1. Conclusions

In order to enhance thermoelectric efficiency, two approaches have been made to increase the number of interfaces hence the amount of phonon boundary scattering. In this thesis, SiGe was chosen for the purpose of power generation for space application. The first approach was heat treatment on SiGe alloy at higher temperature than the solid line of phase diagram. This procedure was expected to melt the alloy slightly and form additional boundaries. Another approach to increase interfaces was SiGe nanocomposite. The SiGe composite was made with nanosized silicon particles; the small grain size was expected to provide more interfaces so that more phonon boundary scattering were expected than composite made with micro-sized silicon particles.

Along with the sample preparation, measurement systems were also developed to produce reliable and fast results. The four probe method was utilized to measure electrical conductivity. And the sample holder was also designed for quick measurement. The

Angstrom method, which determines the thermal conductivity indirectly, was found to be the most reliable method to measure the thermal conductivity. The Borosilicate Pyrex Glass was utilized to calibrate the thermal conductivity measurement, and we got 7% reliability with 7% repeatability.

These measurement systems were used to measure thermoelectric properties of the samples. Reduction in thermal conductivity was observed for both sample preparation methods. For the heat treated SiGe, the thermal conductivity decreased by a factor of two while maintaining the power factor, hence ZT doubled. For the SiGe nanocomposite, the thermal conductivity reduced almost by a factor of four compared to its alloy counterpart. The lowest thermal conductivity value of SiGe nanocomposite, 1.66 W/mK was even comparable with the lowest value ever measured in SiGe superlattices, 1.4 W/mK. Thermal conductivity reduced more in silicon rich nanocomposite than in germanium rich nanocomposite. This trend in thermal conductivity was in good agreement with recent modeling studies on SiGe nanocomposites.

4.2. Future Plans

Although reduction in thermal conductivity was observed by the heat treatment and the nanocomposite approaches, enhancement of ZT was not achieved due to the accompanying reduction in electrical conductivity. Besides, there are not enough modeling studies which can well explain reduction in thermal conductivity of nanocomposite. In this section, uncharted area in nanocomposite study, which remain to be done in near future, are discussed.

4.2.1. Method to Increase the Power Factor

The power factor is determined by the square of the Seebeck coefficient times the electrical conductivity. It is hard to increase the power factor because these two parameters are inversely dependent on each other. With nanostructures, increase in the Seebeck coefficient can be observed without decrease in electrical conductivity by the quantum confinement effect.[4, 5, 20] However, in our study of SiGe nanocomposite, increase in power factor by the quantum confinement effect did not appear. Therefore, proper methods to increase the power factor, especially electrical conduictivity, in SiGe nanocomposite should be explored.

The first approach to achieve high electrical conductivity is to make nanocomposite with different size particles in order to observe the quantum confinement effect. This approach is also useful for achieving low thermal conductivity. The systematic study of hot press conditions to get a dense material should be developed first.

The second approach is to change the composition of SiGe. Silicon and germanium have different energy band structures. Energy band gap and momentum decides energy band structures. If an electron is to be in conduction band, both energy band gap and momentum should be applied to the electron. Silicon and germanium have similar energy band gap but different momentum. When these two materials meet along boundaries, mismatch in momentum hinder electrons from flowing current. Hence, in order to have good electrical conductivity, the energy band structure should be matched. $Si_{1-x}Ge_x$ alloys are known to have "silicon-like" energy band structure when x is less than 0.85.[32] Electrons will not be scattered if composite is made of silicon and SiGe alloys rather than

silicon and germanium.

The third approach is to explore optimum doping concentration to achieve high power factors. This approach also requires study on doping activation. Also, dopants should be activated by normal annealing processes. The temperature to activate the dopants is well known from several semiconductor processing technology.[41]

4.2.2. High Temperature Measurement System

Actual application of thermoelectric power generation requires high temperature. Therefore, it is more important to characterize thermoelectric properties at high temperature than at room temperature. However, high temperature measurement system has never been setup for SiGe nanocomposites study in our laboratory.

High temperature measurement is more challenging than room temperature measurement. The contact between wires and the samples cannot be secured due to low melting temperature of the silver paste. However, Electrical conductivity can be easily measured by the sample holder which was discussed in section 2.2.2. A sample in the sample holder can be put inside of the furnace to reach high temperature ambient, and then the electrical conductivity is measured in the same way as for room temperature measurement. Figure 4.2.1 shows the schematic of high temperature system for the electrical conductivity measurement. The vacuum pump is utilized to evacuate the air to prevent oxidation on the sample. As in the heat treatment case, Argon gas will flow in to push away the remaining of air and to be used as heating-medium. Wires are connected inside and outside of the chamber by a stainless steel feed through at the cap.

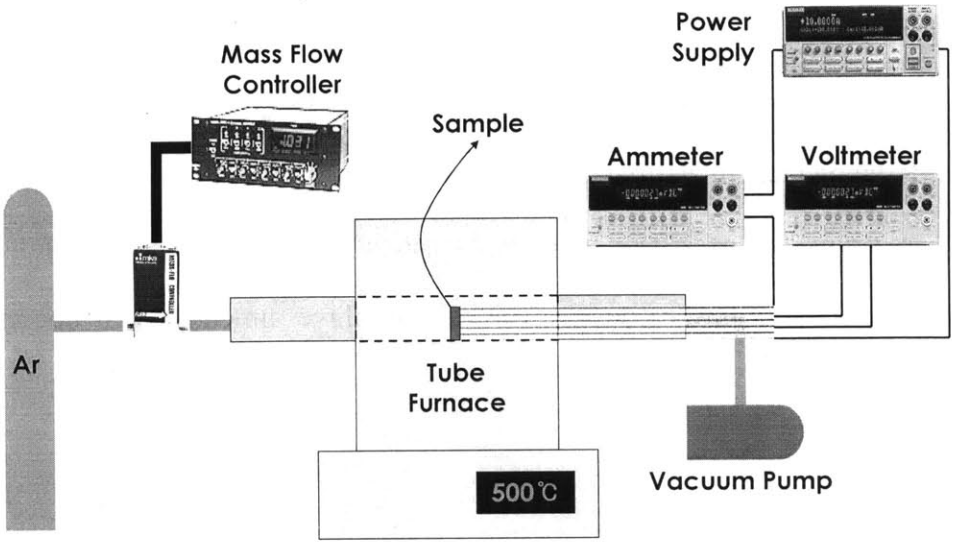

Fig. 4.2.1. A schematic for electrical conductivity measurement at high temperature.

But for the Seebeck coefficient or thermal conductivity, temperature measurement by thermocouples is challenging due to contact problem. Optical detectors can be another choice for temperature measurement. And laser can be used as a power source to produce a temperature gradient. The Laser Flash Method is another well established transient method for thermal conductivity using the laser technique.[42] For the Seebeck coefficient with laser heat source, temperature can be acquired also by optical detectors.

4.2.3. Modeling Study for the Nanocomposites

Since Hicks and Dresselhaus suggested the possible increase in *ZT* of nanostructure,[4] papers regarding modeling of thermoelectric properties in nanostructure have also been published. But most of the modeling studies deal with special kinds of periodic nanostructures such as superlattices or nanowires, which are impratical for large scale production. Although trend of properties with size effect is predictable, there has not been the exact model that can well explain thermal conductivity of nanocomposites. However,

it is quite encouraging that Yang showed a modeling study of thermal conductivity in two dimensional SiGe nanocomposites.[39] He simulated the thermal conductivity of silicon nanowires embedded in germanium host and showed reduction in thermal conductivity with decreasing size of silicon nanowires and with increasing atomic ratio of silicon. There exists need to further develop models for three dimensional nanocomposites and electron transport.

References

1. Nolas, G. S., Sharp, J. & Goldsmid, H. J. Thermoelectrics: Basic Principles and New Materials Developments (Springer, 2001).
2. Rowe, D. M. Handbook of Thermoelectrics (CRC Press, 1995).
3. Chen, G., Dresselhaus, M. S., Dresselhaus, G., Fleurial, J. P. & Caillat, T. Recent developments in thermoelectric materials. International Materials Reviews 48, 45 (2003).
4. Hicks, L. D. & Dresselhaus, M. S. Effect of quantum-well structures on the thermoelectric figure of merit. Physical Review B 47, 12727 (1993).
5. Hicks, L. D. & Dresselhaus, M. S. Thermoelectric figure of merit of a one-dimensional conductor. Physical Review B 47, 16631 (1993).
6. Colvard, C. et al. Folded Acoustic and Quantized Optics Phonons in (GaAl)As Superlattices. Physical Review B 31, 2080 (1985).
7. Narayanamurti, V., Stormer, H. L., Chin, M. A., Gossard, A. C. & Wiegmann, W. Selective Transmission of High-Frequency Phonons by a Superlattice: the "Dielectric" Phonon Filter. Physical Review Letters 43, 2012 (1979).
8. Tamura, S., Hurley, D. C. & Wolfe, J. P. Acoustic-Phonon Propagation in Superlattices. Physical Review B 38, 1427 (1989).
9. Chen, G. Phonon Wave Heat Conduction in Thin Films and Superlattices. Journal of Heat Transfer 121, 945 (1999).
10. Hyldgaard, P. & Mahan, G. D. Phonon Superlattice Transport. Physical Review B 56, 10754 (1997).
11. Borca-Tasciuc, T. et al. Thermal conductivity of symmetrically strained Si/Ge

superlattices. Superlattices and Microstructures 28, 199 (2000).

12. Lee, S. M., Cahill, D. G. & Venkatasubramanian, R. Thermal conductivity of Si-Ge superlattices. Applied Physics Letter 70, 2957 (1997).
13. Liu, W. L., Borca-Tasciuc, T., Chen, G., Liu, J. L. & Wang, K. L. Anisotropy thermal conductivity of Ge-quantum dot and symmetrically strained Si/Ge superlattice. Journal of Nanoscience and Nanotechnology 1, 39 (2001).
14. Yang, B. & Chen, G. Lattice dynamics study of anisotropic heat conduction in superlattices. Microscale Thermophysical Engineering 5, 107 (2001).
15. Chen, G. Size and interface effects on thermal conductivity of superlattices and periodic thin-film structures. Journal of Heat Transfer 119, 220 (1997).
16. Chen, G. Thermal conductivity and ballistic-phonon transport in the cross-plane direction of superlattices. Physical Review B 57, 14958 (1998).
17. Chen, G. & Neagu, M. Thermal conductivity and heat transfer in superlattices. Applied Physics Letter 71, 2761 (1997).
18. Ren, S. Y. & Dow, J. D. Thermal Conductivity of Superlattice. Physical Review B 25, 3750 (1982).
19. Harman, T. C., Taylor, P. J., Walsh, M. P. & LaForge, B. E. Quantum dot superlattice thermoelectric materials and devices. Science 297, 2229 (2002).
20. Hicks, L. D., Harman, T. C., Sun, X. & Dresselhaus, M. S. Experimental study of the effect of quantum-well structures on the thermoelectric figure of merit. Physical Review B 53, 10493 (1996).
21. Venkatasubramanian, R., Silvola, E., Colpitts, T. & O'Quinn, B. Thin-film thermoelectric devices with high room-temperature figures of merit. Nature 413, 597 (2001).
22. Yang, B., Liu, J., Wang, K. & Chen, G. in International Conference on Thermoelectrics 344 (2001).
23. Campbell, M. R. & Hogarth, C. A. A correction to the theory of Harman's method of determining the thermoelectric figure of merit. International Journal of Electronics 19, 571 (1965).

24. Harman, T. C. Special techniques for measurement of thermoelectric properties. Journal of appl. phys. 29, 1373 (1958).

25. Vandersande, J. W., Wood, C. & Draper, S. in Material Research Society 347 (1987).

26. Goldsmid, H. J. The Electric Conductivity and Thermoelectric Power of Bismuth Telluride. Proc. Phys. Soc. 71, 633 (1958).

27. Sze, S. M. Physics of Semiconductor Devices (Wiley Inter-Science, 1981).

28. Tritt, T. M. & Browning, V. M. Overview of measurement and characterization techniques for thermoelectric materials (ed. Tritt, T. M.) (Semiconductors and Semimetals, 2001).

29. Incropera, F. P. & DeWitt, D. P. Fundamentals of Heat and Mass Transfer (Wiley, 1996).

30. Maglic, K. D., Cezairliyan, A. & Peletsky, V. E. Compendium of Thermophysical Property Measurement Methods (Plenum Press, 1984).

31. Carslaw, H. S. & Jaeger, J. C. Conduction of Heat in Solids (Oxford University Press, 1947).

32. Levinshtein, M. E., Runyantsev, S. L. & Shur, M. S. Properties of Advanced Semiconductor Materials: GaN, AlN, InN, BN, SiC, SiGe (Wiley, 2001).

33. Kittel, C. Introduction to Solid State Physics (Wiley, 1996).

34. Angstrom, A. J. Neue Methode des Warmeleitungsvermogen der Korper zu bestimmen. Ann. Phys. Chem. 114, 513 (1861).

35. Abeles, B., Cody, G. D. & Beers, D. S. Apparatus for the measurement of the thermal diffusivity of solids at high temperatures. Journal of Applied Physics 31, 1585 (1960).

36. King, R. W. A method of measuring heat conductivities. Physical Review 6, 437 (1915).

37. Sidles, P. H. & Danielson, G. C. Thermal diffusivity of metals at high temperatures. Journal of Applied Physics 25, 58 (1954).

38. Song, D. & Chen, G. Thermal conductivity of periodic microporous silicon films. Applied Physics Letter 84, 687 (2004).

39. Yang, R. & Chen, G. Thermal conductivity modeling of periodic two-dimensional nanocompoites. Physical Review B 69, 195316 (2004).

40. Dames, C. & Chen, G. in Material Research Society (eds. Nolas, G. S., Yang, J., Hogan, T. P. & Johnson, D. C.) (2003).

41. Plummer, J. D., Deal, M. D. & Griffin, P. B. Silicon VLSI Technology: Fundamentals, Practice and Modeling (Prentice Hall, 2000).

42. Parker, W. J., Jenkins, R. J., Butler, C. P. & Abbott, G. L. Flash method of determining thermal diffusivity, heat capactity, and thermal conductivity. Journal of appl. phys. 32, 1679 (1961).